

**SCHOTTKY AND POOLE-FRENKEL CONDUCTION
MECHANISMS IN ZRON/SIC SYSTEM**

VANESSA LUSUS

**FACULTY OF ENGINEERING
UNIVERSITY OF MALAYA
KUALA LUMPUR**

2020

**SCHOTTKY AND POOLE-FRENKEL CONDUCTION
MECHANISMS IN ZRON/SIC SYSTEM**

VANESSA LUSUS

**RESEARCH PROJECT SUBMITTED IN PARTIAL
FULFILMENT OF THE REQUIREMENTS FOR THE
DEGREE OF MASTER OF MECHANICAL
ENGINEERING**

**FACULTY OF ENGINEERING
UNIVERSITY OF MALAYA
KUALA LUMPUR**

2020

UNIVERSITY OF MALAYA
ORIGINAL LITERARY WORK DECLARATION

Name of Candidate: VANESSA LUSUS

Matric No: 17202632

Name of Degree: Master of Mechanical Engineering

Title of Project Paper/Research Report/Dissertation/Thesis (“this Work”):

Schottky and Poole-Frenkel Conduction Mechanisms in ZrON/SiC system

Field of Study:

I do solemnly and sincerely declare that:

- (1) I am the sole author/writer of this Work;
- (2) This Work is original;
- (3) Any use of any work in which copyright exists was done by way of fair dealing and for permitted purposes and any excerpt or extract from, or reference to or reproduction of any copyright work has been disclosed expressly and sufficiently and the title of the Work and its authorship have been acknowledged in this Work;
- (4) I do not have any actual knowledge nor do I ought reasonably to know that the making of this work constitutes an infringement of any copyright work;
- (5) I hereby assign all and every rights in the copyright to this Work to the University of Malaya (“UM”), who henceforth shall be owner of the copyright in this Work and that any reproduction or use in any form or by any means whatsoever is prohibited without the written consent of UM having been first had and obtained;
- (6) I am fully aware that if in the course of making this Work I have infringed any copyright whether intentionally or otherwise, I may be subject to legal action or any other action as may be determined by UM.

Candidate’s Signature

Date: 15/09/2020

Subscribed and solemnly declared before,

Witness’s Signature

Date: 15/09/2020

Name:

Designation:

SCHOTTKY AND POOLE-FRENKEL CONDUCTION MECHANISMS IN ZrON/SiC SYSTEM

ABSTRACT

In this work, the conduction mechanisms of Schottky Emission (SE) and Poole-Frenkel (PF) Emission for the ZrON/SiC system with a temperature range between 400 °C to 900 °C were analyzed. Understanding of the conduction charge mechanisms will help to estimate leakage characteristics of the ZrON/SiC system. Based on the J-E plot measured at different temperatures for 15 minutes, the obtained r^2 was ranged between 0.90–0.98, which confirmed the data obtained complied with the standard SE model. Furthermore, the data plotted from the Effective Barrier Height Extracted from the SE plot showed the highest values of ϕ_B (1.19 eV) were achieved. Thus, based on the data analyzed, both the ϕ_B and k_r values reduces as the measured temperature increases. Meanwhile, the calculated J-E data and the modelled PF emission curves for the ZrON/SiC system showed that the sample at a temperature of 500 °C has the highest k_r of 3.03. Additionally, the refractive index obtained by the electrical method is similar to the one obtained by the optical measurement, with r^2 of 0.90-0.99. Based on the data tabulated for both SE and PF, it can be inferred that an increase in temperature will increase the interfacial layer (IL) which will result in a decrease in dielectric strength.

Keywords: Conduction charge mechanism, Schottky Emission, Poole-Frenkel Emission, Zirconium Oxynitride (ZrON), Silicon Carbide (SiC)

MEKANISMA PENGALIRAN PANCARAN SCHOTTKY DAN POOLE-FRENKEL DI DALAM SISTEM ZrON/SiC

ABSTRAK

Di dalam kertas kerja ini, mekanisme pengaliran pancaran Schottky (SE) dan Poole-Frenkel (PF) untuk sistem ZrON/SiC, dengan julat suhu di antara 400 °C hingga 900 °C, telah dianalisis. Memahami mekanisme pengaliran cas arus akan membantu untuk menganggarkan ciri kebocoran arus untuk sistem ZrON/SiC. Berdasarkan plot J-E yang diukur pada suhu yang berbeza selama 15 minit, r^2 di anantara julat 0.90-0.98 telah diperolehi dan ini mengesahkan data yang didapati padan dengan model SE standard. Selanjutnya, data yang diplot dari Sawar Tinggi Berkesan yang diekstrak dari plot SE menunjukkan nilai tertinggi ϕ_B (1.19 eV) telah dicapai. Oleh itu, berdasarkan data yang dianalisis, kedua-dua nilai ϕ_B dan k_r akan berkurangan ketika suhu yang diukur meningkat. Sementara itu, data J-E yang dihitung dan keluk pelepasan PF yang dimodelkan untuk sistem ZrON / SiC menunjukkan bahawa sampel pada suhu 500 °C mempunyai k_r tertinggi iaitu 3.03. Selain itu, indeks biasan yang diperolehi dengan kaedah elektrik padan dengan maklumat pengukuran optik, dengan r^2 0.90-0.99. Kesimpulannya, berdasarkan data yang dijabarkan untuk kedua-dua SE dan PF, peningkatan suhu akan meningkatkan lapisan antara muka (IL) dan seterusnya akan mengakibatkan penurunan kekuatan dielektrik.

Kata kunci: Mekanisma pengaliran caj arus, pancaran Schottky (SE), pancaran Poole-Frenkel (PF), Karbida Silicon (SiC), Oksinitrid Zirkonium (ZrON)

ACKNOWLEDGEMENTS

Firstly, praise to God for all the blessings as I was able to successfully complete my dissertation entitled “Schottky and Poole-Frenkel Conduction Mechanisms in ZrON/SiC System”. Next, I would like express my deepest gratitude to my supervisor, Prof. Madya IR Dr. Wong Yew Hoong, for his constant guidance and willingness to share his vast knowledge which enables me to understand more about this project and its manifestations in great depths. Besides that, I would like to express very great appreciation to my friends for their valuable and constructive suggestions during the planning and development of my dissertation and they were always there cheering me up through euphoria and bad times. Their willingness to give their time so generously has been very much appreciated. Lastly, special thanks to my sisters and parents, for their continuous support and encouragement throughout my journey in completing my Master’s Degree in University of Malaya.

TABLE OF CONTENTS

Abstract	iii
Abstrak	iv
Acknowledgements	v
Table of Contents	vi
List of Figures	viii
List of Tables	ix
List of Symbols and Abbreviations	x
List of Appendices	xii
CHAPTER 1: INTRODUCTION	1
1.1 Background of Study	1
1.2 Problem Statement.....	4
1.3 Objectives.....	4
1.4 Scope of Study.....	5
CHAPTER 2: LITERATURE REVIEW	6
2.1 Wide Bandgap (WBG) Material.....	6
2.1.1 Wide Bandgap Devices	6
2.1.2 SiC WBG Devices and Characteristics	7
2.1.2.1 Structural and Physical Properties of SiC.....	7
2.1.2.2 Optical and Electronic Properties of SiC.....	9
2.1.2.3 Hardness and Mechanical Properties of SiC.....	10
2.1.2.4 Applications of Silicon Carbide Devices.....	11
2.2 Gate Oxide.....	13
2.2.1 Zirconium Oxynitride as Alternative High K Material.....	14

2.2.2	Role of Nitrogen in Gate Oxides on Si and SiC Substrates	15
2.3	Conduction Mechanisms in Dielectric Material.....	15
2.3.1	Electrode-limited Conduction Mechanisms	16
2.3.2	Schottky or Thermionic Emission	17
2.3.3	Bulk-Limited Conduction Mechanisms	18
2.3.4	Poole-Frenkel Emission	18
CHAPTER 3: METHODOLOGY		21
3.1	Introduction.....	21
3.2	Experimental Flow Chart.....	22
3.3	Starting Materials	23
3.4	SiC Substrate Preparation	23
3.5	Formation of Zr-Oxynitride Thin Film on SiC Substrate	23
3.6	Characterization and Testing.....	24
3.6.1	Electrical Properties.....	24
CHAPTER 4: RESULTS & DISCUSSION		25
4.1	Oxidation and Nitridation Mechanisms	25
4.2	Electrical Characterizations.....	28
4.2.1	Current Density-Electric Field (J-E) Characteristics and Charge Conduction Mechanisms	28
CHAPTER 5: CONCLUSION		37
5.1	Summary	37
5.2	Recommendations for Future Project	37
List of Publications and Papers Presented.....		38
REFERENCES		39

LIST OF FIGURES

Figure 2.1: Summary of Si, SiC and GaN relevant material properties (Wang et al., 2018)	7
Figure 2.2: Schematic Energy Band Diagram of Poole-Frenkel emission in MIS (Chiu, 2014)	19
Figure 2.3: Schematic Energy Band Diagram of Schottky emission in MIS (Chiu, 2014)	20
Figure 3.1 : Experimental Flow Chart (Wong & Cheong, 2011)	22
Figure 4.1 : SE Plot (J-E Plot Measured at Different Temperatures for 15 minutes).....	29
Figure 4.2 : Effective Barrier Height Extracted from SE plot.....	30
Figure 4.3 : Dynamic Dielectric Constant Extracted from SE Plot	31
Figure 4.4 : The measured J-E Data and Modelled PF Emission Curves for ZrON/SiC System.....	32
Figure 4.5 : Dynamic Dielectric Constant Extracted versus Temperature based on PF Emission Plot.....	33
Figure 4.6 : Relationship between Leakage Current Density and Electrical Field for Various Temperature within the Range of 400 ⁰ C – 900 ⁰ C	35
Figure 4.7 : Relationship between Leakage Current Density and Electrical Field for Temperature at 400 ⁰ C	36

LIST OF TABLES

Table 1.1 : Basic Properties of Semiconductor Materials (Marckx et al., 2006).....	2
Table 2.1 : The Lattice Constants (\AA) of SiC Polytypes at Room Temperature (Levinshtein et al., 2001)	8
Table 2.2 : Physical Properties of SiC (Fraga et al., 2015).....	9
Table 2.3 : Properties of Various Semiconductor (Baliga, 2018)	10
Table 2.4 : Mechanical Properties of SiC and Si (Marckx et al., 2006)	11
Table 2.5 : SiC Devices and Applications	12
Table 2.6 : Dielectric and their respective Dielectric Constant Value (Kim et al., 2011; Wong & Cheong, 2010).....	14
Table 4.1 : Dynamic Dielectric Constant from Gradient $\ln (J/E) - E^{1/2}$ Plot Fitted with Poole-Frenkel Emission as a Function of Oxidation and Nitridation Temperature	33

LIST OF SYMBOLS AND ABBREVIATIONS

C	:	Diamond
CTE	:	Coefficients of thermal expansion
EOT	:	Equivalent oxide thickness
eV	:	Electron volt
GaN	:	Gallium Nitride
HF	:	Hydrofluoric
IL	:	Interfacial layer
k	:	Dielectric
MIS	:	Metal-insulator-structure
MOS	:	Metal-oxide semiconductors
N ₂ O	:	Nitrous oxide
PF	:	Poole-Frenkel
SE	:	Schottky Emission
Si	:	Silicon
SiC	:	Silicon Carbide
SiO ₂	:	Silicon Dioxide
ZrO ₂	:	Zirconium Oxide
ZrON	:	Zirconium Oxynitride
WBG	:	Wide bandgap
Å	:	Angstrom
°C	:	Degree Celsius
Ω	:	Ohm

University of Malaya

LIST OF APPENDICES

Appendix A: Example

7

.....

University of Malaya

University of Malaya

CHAPTER 1: INTRODUCTION

1.1 Background of Study

The advancement of semiconductor materials and devices has been a significant engine for numerous progressive changes in modern society. High-temperature electronics is an area that holds great promise in wide bandgap (WBG) semiconductors. Power electronics involves the conversion of electric power using power semiconductor devices and circuits. Hence, the utilization of high-performance power devices will greatly improve the energy-saving capability of a device.

Over several decades, power-semiconductor devices made of bandgap-energies larger than in Si have been extensively researched. Some of the properties of semiconductor materials are given in Table 1.1. The GaN, SiC (4H), and C (diamond) are the best semiconductor material to create future power-electronic devices (Hudgins, 2003). Among these three materials, diamond has the highest thermal conductivity, bandgap, and electron mobility. However, there are two aspects of C (diamond) that make it less than ideal. First, the manufacturing technology for the material and devices is less developed and mature than SiC and GaN. Secondly, the CTE for C (diamond) is very low. Thus, the GaN and SiC are by comparison to C (diamond) very well suited to conventional package materials and provide a better thermomechanical match than Si.

Table 1.1 : Basic Properties of Semiconductor Materials (Marceckx et al., 2006)

Material	Bandgap Energy (eV)	Breakdown Field (MV/cm)	Electron Mobility (cm²/V·s)	Electron Drift V_{sat} (cm/s)	Thermal Conductivity (W/m/K)
Si	1.12	0.6	1100	1.0 x 10 ⁷	150
GaAs	1.42	0.6	6000	8.0 x 10 ⁷	50
GaN	3.39	3.3	1000	2.5 x 10 ⁷	130
3C-SiC	2.2	2	750	2.5 x 10 ⁷	500
4H-SiC	3.26	3	800	2.0 x 10 ⁷	490
6H-SiC	3	3.2	370	2.0 x 10 ⁷	490
Diamond	5.5	6	2200	2.7 x 10 ⁷	2000

Silicon carbide (SiC) has superior physical properties thus making it a promising material for advanced power devices. GaN is also desirable as a power device and is very close to SiC's intrinsic potential. Today, however, the SiC technology growth and devices are more advanced, and SiC power devices yield better performance and more reliable.

The integration of functional gate oxides on wide bandgap (WBG) semiconductors is of interest to realize next generation metal-oxide semiconductors (MOS) for high-power and high-radiation applications. In order to fabricate these devices, the gate oxide must be able to bear a high transverse electric field and be of excellent reliability, so that the leakage current through the gate oxide could be minimized (Wong & Cheong, 2012). Therefore, high-dielectric-constant materials have attracted a great deal of attention from industries as the alternative to conventional SiO₂ gate dielectrics. Of numerous high-*k* gate oxides, ZrO₂ has attracted much attention owing to its fascinating properties such as high-dielectric-constant value (22–25), large energy bandgap (5.8 –7.8 eV), etchability in hydrofluoric (HF) solution, and thermal stability in contact with silicon (Wong & Cheong, 2012; Nieh et al., 2003).

Although ZrO_2 is thermally stable with Si, oxygen diffusion during thermal processing can result in interfacial layer (IL) growth which leads to equivalent oxide thickness (EOT) increase (Busch et al., 2000). Nieh et al. (2003) had reported that the increase in EOT during MOS devices fabrication can be prevented by introducing two forms of nitrogen incorporation in the ZrO gate stack - Si surface nitridation prior to ZrO deposition and Zr-oxynitride. Additionally, in research by Wong and Cheong (2012), the electrical properties of MOS devices can be improved via simultaneous thermal oxidation and nitridation sputtered Zr on Si using N_2O gas.

The comprehension of the electronic conduction mechanism is critical because it strongly affects the properties of the device. The type of electronic conduction mechanism depends on a variety of variables, in particular on the nature of metallic contact (either ohmic or blocking), the voltage level and the voltage applied across the sample, surface roughness, grain size and its temperature (Chenari et al., 2011). The methods for characterizing these conduction mechanisms is important, as multiple conduction mechanisms can simultaneously contribute to the conduction current through the dielectric film. In dielectric films, there are two kinds of mechanisms of conduction, that is, electrode-limited conduction mechanism and bulk-limited conduction mechanism. However, for this study, we only examined two types of conduction mechanism in ZrON/SiC system, which are the Schottky and Poole-Frenkel emission mechanisms.

1.2 Problem Statement

- Interface trap has a significant impact on the reliability and lifetime of a MOS device, as it is a major source to leakage current. Thus, the leakage characteristic should be thoroughly studied as it is one of the critically electrical properties.
- Understanding the charge conduction mechanisms will help to estimate leakage characteristics of the material and also to realize a highly reliable device.

1.3 Objectives

1. To investigate the possible presence of Schottky and Poole-Frenkel emission mechanisms in ZrON/SiC system.
2. To compute and to compare the dynamic dielectric constants in the oxynitride material caused by Schottky and Poole-Frenkel emission mechanisms in ZrON/SiC system.

1.4 Scope of Study

Zirconium Oxynitride (ZrON) thin film on SiC substrate can be formed by simultaneous oxidation and nitridation in nitrous oxide sputtered Zr on SiC. The oxidation and nitridation of the sputtered Zr on SiC substrate were carried out in nitrous oxide (N₂O) ambient for 15 minutes at various temperatures (400-900°C). The effect of temperature on the type of conduction mechanism were studied and investigated.

University of Malaya

CHAPTER 2: LITERATURE REVIEW

2.1 Wide Bandgap (WBG) Material

2.1.1 Wide Bandgap Devices

Wide Bandgap material is a type of material having electronic energy band gaps which are substantially greater than one electron volt (eV) (Wang et al., 2018). WBG materials display various features that make it attractive for power electronic converters compared to the narrow bandgap Si. In general, the energy difference, electrical field breakdown, thermal conductance, melting points and electron speed are all considerably greater for WBG materials (Wang et al., 2018). Such features allow WBG semiconductor-based power devices to work at much higher voltage, frequency of switching and temperature than Si. WBG's electron saturated drift speed is higher than that of Si, resulting in an improvement in WBG devices switching power. The high thermal conductivity also allows the dissipated heat of WBG units to be removed from the device easily. A higher power can therefore be handled by the device at a given junction temperature. In summary, WBG-based power devices offer low specific on-state resistance, fast switching speed, high operating temperature and voltage capabilities (Millan et al., 2014).

There are many III–V and II–VI compound semiconductors with large bandgaps. Among the possible WBG semiconductor material candidates, SiC and GaN show the best compromise of theoretical characteristics such as high blocking voltage capability, high-temperature operation, and high switching speed, and maturity of their technological processes

(Millan et al., 2014). Figure 2.1 highlights some key material properties of WBG semiconductors candidates to replace Si.

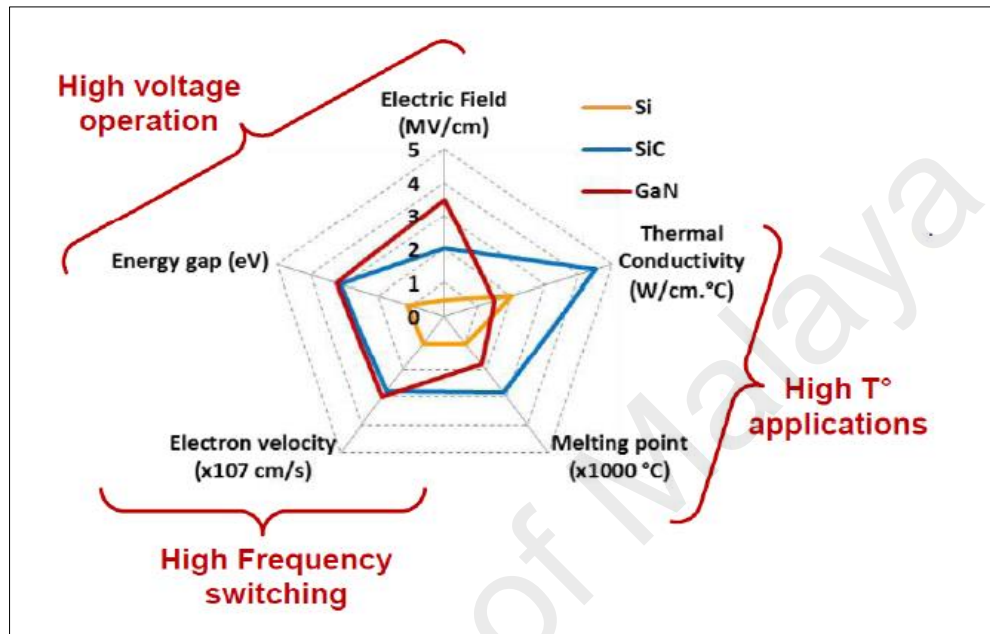


Figure 2.1: Summary of Si, SiC and GaN relevant material properties (Wang et al., 2018)

2.1.2 SiC WBG Devices and Characteristics

2.1.2.1 Structural and Physical Properties of SiC

Silicon carbide, also known as Carborundum, is an IV-IV compound material of Silicon and Carbon. A distinctive property of SiC is its polytypism. Polytypism is the phenomenon

where a material can adopt different crystal structures which vary in one dimension without changes in chemical composition (Kimoto & Cooper, 2014).

In SiC compound, Si and C atoms are tetravalent elements and have four valence electrons in their outermost shells. Both Si and C atoms are tetrahedrally bonded with covalent bonds by sharing electron pairs in sp^3 -hybrid orbitals to form a SiC crystal (Kimoto & Cooper, 2014). Thus, due to the strong Si-C bond, SiC exhibit high bond energy which is 4.6 eV (Kimoto & Cooper, 2014).

Different SiC polytypes will exhibit different lattice constants due to the dissimilarity of the crystal structures of each polytypes. However, despite the variance in crystal structures of each polytypes, all SiC polytypes possess nearly equivalent Si-C bond length (1.89 Å) (Levinshtein et al., 2001). Table 2.1 shows the characteristic dimensions of crystalline meshes of SiC-3C, SiC-4H, SiC-6H at room temperature. The other physical properties of SiC are summarized in Table 2.2 as well.

Table 2.1 : The Lattice Constants (Å) of SiC Polytypes at Room Temperature (Levinshtein et al., 2001)

Polytype	A (Å)	C (Å)
3C	4.3596	-
4H	3.0798	10.0820
6H	3.0805	15.1151

Table 2.2 : Physical Properties of SiC (Fraga et al., 2015)

Physical Properties of SiC	Appearance	Black gray to green powder, gray solid
	Odour	Odourless
	Solubility	Insoluble in water, alcohol and acid
	Density	3.21 g/cm ³
	Melting Point	~2800 °C

2.1.1.2.2 Optical and Electronic Properties of SiC

The optical and electronic properties of SiC greatly depends on the type of polytype as different polytype will yield different electronic band structures due to the variance in its periodic potential. In many device applications, SiC's exceptionally high breakdown field, wide bandgap energy, high carrier saturation velocity, and high thermal conductivity could enable substantial performance gains, greatly overcoming non-trivial low-field carrier mobility disadvantages (Wondrak et al., 2001). A high breakdown electric field allows the design of SiC power devices with thinner and higher doped blocking devices (Singh, 2006). Furthermore, the wider bandgap and higher thermal conductivity of SiC relative to Si allows the device to be operated at higher temperature and also larger power can be applied to the devices (Singh, 2006).

The electrical properties of the more common SiC polytypes are compared to the properties of Silicon and GaAs in Table 4. SiC possesses a much higher thermal conductivity than GaAs at a temperature as high as 300 K as well as a band gap of approximately twice the band gap of GaAs. The band gap of Si, GaAs and of 6H-SiC are about to 1.1 eV, 1.4 eV and 2.9 eV respectively. Additionally, based on the information provided at Table 2.3, it can be seen that different SiC polytypes will have different property, such as 4H-SiC exhibit wider energy bandgap, and higher electron and hole mobility compared to 6H-SiC.

Table 2.3 : Properties of Various Semiconductor (Baliga, 2018)

Property	6H-SiC	4H-SiC	GaN	GaAs	Si
Energy Bandgap (eV)	2.9	3.26	3.39	1.43	1.12
Electric field Breakdown (x10 ⁶ V/cm @ 1kV operation)	2.5	2.2	3.0	0.30	0.25
Dielectric Constant	9.6	9.7	9.0	12.8	11.8

2.1.2.3 Hardness and Mechanical Properties of SiC

Silicon carbide (SiC) is the third hardest material after diamond and boron nitride, which gives SiC its excellent properties such as high-temperature stability, imperviousness to chemical attack, and biological compatibility (Davis, 2017). Table 2.4 displays the key mechanical properties of SiC and Si. The hardness and Young's modulus of SiC are much higher than those of Si. The yield (fracture) strength of SiC is as high as 21 GPa at room

temperature meanwhile for Si, the fracture strength is 7 GPa at room temperature. Since SiC polytypes consist of similar Si-C links, SiC of various polytypes can maintain their high hardness and elasticity even at very high temperatures.

Table 2.4 : Mechanical Properties of SiC and Si (Marcckx et al., 2006)

Properties	4H- or 6H-SiC	Si
Young's Modulus (GPa)	390-90 GPa	160
Fracture Strength (GPa)	21	7

2.1.2.4 Applications of Silicon Carbide Devices

Silicon Carbide is a significant non-oxide ceramic which has many industrial applications. It has exclusive properties like high toughness and strength, chemical and thermal stability, high melting point and oxidation resistance (Gerhardt, 2011). All these qualities make SiC an excellent candidate for high-performance and high temperatures electronic devices. Moreover, due to its large bandgap, high thermal stability and resistance to corrosion, SiC is a technology which enables many applications that conventional semiconductors cannot serve such as high-power microwave devices, high-temperature electronics for automotive (Kimoto & Cooper, 2014), and gas or chemical sensors for internal combustion boilers or engines (Gerhardt, 2011). Table 2.5 lists the various types of SiC devices and their application.

Table 2.5 : SiC Devices and Applications

Application	Example of Device
<p>Microwave Device (Kimoto & Cooper, 2014)</p>	<ul style="list-style-type: none"> ➤ Static Induction Transistors (SITs) - SiC can support higher voltages ΔV than silicon or GaAs due to its higher critical field. ➤ Impact Ionization Avalanche Transit-Time (IMPATT) Diodes
<p>High Temperature Integrated Circuit (Kimoto & Cooper, 2014)</p>	<ul style="list-style-type: none"> ➤ SiC is appropriate for high-temperature environment. For example, in automobiles powered by internal combustion engines, the placement of sensors and control electronics directly on the engine can lead to increased efficiencies and lower emissions.
<p>Sensors (Choyke et al., 2013)</p>	<ul style="list-style-type: none"> ➤ Micro-Electro-Mechanical Sensors (MEMS) <ul style="list-style-type: none"> - The excellent mechanical properties and high temperature capability of SiC makes it suitable for MEMS device. - SiC MEMs suitable for biofiltration applications due to its biocompatibility, and resistance to biofouling. ➤ Gas Sensor <ul style="list-style-type: none"> - The wide band-gap of silicon carbide, 3.2 eV for 4H-SiC, permits an operation temperature up to 1000°C, with time constants for the gas response of a few milliseconds. ➤ Optical Detector <ul style="list-style-type: none"> - The wide bandgap of SiC makes it transparent to visible light, since photons in the visible spectrum have energies less than the bandgap and are not absorbed. Thus, making it ideal for ultraviolet photodetectors such as pin photodiodes and avalanche photodiodes (APDs).

2.2 Gate Oxide

Gate-oxide degradation is more critical in SiC-SiO₂ structure than in Si-SiO₂ structure (Karki & Peng, 2018). This is because of the smaller gate-oxide thickness and the higher electric field that develops across the thinner gate oxide in SiC MOSFETs (Karki & Peng, 2018). Moreover, the existence of oxygen vacancy related defects can influence the electrical interface due to the charge trapping process occurred from these defects.

Many high-dielectric-constant (high-*k*) materials, are currently considered as the potential gate dielectrics to replace conventional SiO₂ in MOS technology due to the problems of high gate leakage current, standby power consumption and gate oxide reliability. The high-*k* films can provide similar capacitance with a physically larger thickness and therefore can be used to reduce the gate leakage current. Among the high-*k* dielectrics being studied, praseodymium oxide (Pr₂O₃) (Chiu et al., 2009), Cerium oxide (CeO₂) (Kim et al., 2011), HfO₂ and Zirconium Oxynitride (ZrON) are promising candidate because of its low leakage current density, good thermal stability large electron effective mass, large band gap, and large dielectric strength. One major disadvantage of CeO₂ is high hysteresis. On the other hand, the drawback of HfO₂ is that, due to the high concentration of electronically active defects found in the material, this can lead to bias stress instability and reliable problems. The list of some common dielectrics and their respective dielectric constant value are shown in Table 2.6.

Table 2.6 : Dielectric and their respective Dielectric Constant Value (Kim et al., 2011; Wong & Cheong, 2010)

Dielectric	Dielectric Constant
Silicon Dioxide (SiO ₂)	3.9
Silicon Nitride (Si ₃ N ₄)	7
Aluminium Oxide (Al ₂ O ₃)	~10
Hafnium Oxide (HfO ₂)	~20
Zirconium Oxide (ZrO ₂)	~23

The desired characteristics of a good high k dielectric are high dielectric strength, high resistance to hot carrier damage and long lifetime under standard operating environment. Furthermore, the bandgap and band offset also play a significant role in describing the characteristics of an excellent high k material. Higher k materials will typically have a lower bandgap than SiO₂. A high k material usually will have k within the range of 25-30. However, the primary concern regarding low bandgap and band offset is that the leakage current will increase due to the tunneling through the barrier. Thus, the high k material needs to offer a good balance between dielectric constant, chemical stability, bandgap, and band offset.

2.2.1 Zirconium Oxynitride as Alternative High K Material

Transition metal oxynitrides and in particular zirconium oxynitrides (ZrO_xN_y) have attracted considerable interest in a wide range of applications. Zirconia film has been opted as one of the alternative materials for gate dielectrics due to its excellent properties such as low

thermal conductivity, a relatively high dielectric constant, high refractive index, high transparency in the visible and near-infrared region, and extreme chemical inertness.

2.2.2 Role of Nitrogen in Gate Oxides on Si and SiC Substrates

The oxidation and/or post oxidation annealing in a nitrogen-containing ambient has greatly enhanced the MOS characteristics and the oxide-SiC interface quality as this process helped in the removal of carbon and passivation of silicon dangling bonds (Feng, 2013). Various research had been conducted to study the effects of thermal oxidation and nitridation of sputtered Zr/Si system in ambient N₂O on its chemical, structural, electronic and electrical properties. Based on the X-ray photoelectron spectrometer results, it has been reported that bulk ZrO₂ and interfacial layer (IL) of Zr-silicate oxynitride (ZrSiON) had formed on the Si substrate. Meanwhile, when a similar method was applied on a sputtered Zr/SiC system, Zr-oxynitride film of Zr-O, Zr-N, and/or Zr-O-N and its interfacial layer consisted of mixed Zr-O, Zr-N, Zr-O-N, Zr-Si-O, Si-N, and/or C-N compounds were identified (Wong & Cheong, 2012).

2.3 Conduction Mechanisms in Dielectric Material

The conduction mechanisms in dielectric films are crucial to the successful applications of dielectric materials. In dielectric film, there are two types of conduction mechanisms: electrode-limited conduction mechanism and bulk-limited conduction mechanism. In general,

the conduction mechanism in dielectric films may be influenced by the following factors: temperature, electric field, stress condition, device structure, electrode material, type of film, film thickness, and deposition method.

2.3.1 Electrode-limited Conduction Mechanisms

The electrode-limited conduction mechanisms depend on the electrical properties at the electrode-dielectric contact. The most important parameter in this type of conduction mechanism is the barrier height at the electrode dielectric interface. The electrode-limited conduction mechanisms include:

- (1) Schottky or thermionic emission
- (2) Fowler-Nordheim tunneling
- (3) Direct tunneling
- (4) Thermionic-field emission.

The current due to thermionic emission is highly dependent on the temperature, whereas the tunneling current is nearly temperature independent. Aside from the barrier height at the electrode-dielectric interface, the effective mass of the conduction carriers in dielectric films is also a key factor in the electrode-limited conduction mechanisms.

2.3.2 Schottky or Thermionic Emission

Schottky emission is a conduction mechanism that if the electrons can obtain enough energy provided by thermal activation, the electrons in the metal will overcome the energy barrier at the metal dielectric interface to go to the dielectric. The energy barrier height at the metal dielectric interface may be lowered by the image force. The barrier-lowering effect due to the image force is called Schottky effect. Thermionic emission is one of the most often observed conduction mechanism in dielectric films, especially at relatively high temperature. The expression of Schottky emission is (Wong & Cheong, 2010):

$$J = A^* T^2 \exp \left[\frac{-q (\phi_B - \sqrt{qE/4\pi\epsilon_r\epsilon_0})}{kT} \right],$$

$$A^* = \frac{4\pi q k^2 m^*}{h^3} = \frac{120 m^*}{m_0},$$

J	: Current density	q	: Electronic charge
A*	: Effective Richardson constant	$q\phi_B$: Schottky barrier height (conduction band offset)
m_0	: Free electron mass	E	: Electric field across the dielectric
m^*	: Effective electron charge in dielectric	k	: Boltzmann's constant
T	: Absolute temperature	h	: Planck's constant
ϵ_0	: Permittivity in vacuum		
ϵ_r	: Optical dielectric constant		

2.3.3 Bulk-Limited Conduction Mechanisms

The bulk-limited conduction mechanisms depend on the electrical properties of the dielectric itself. The most important parameter in this type of conduction mechanism is the trap energy level in the dielectric films. The bulk-limited conduction mechanisms include:

- (1) Poole-Frenkel emission
- (2) Hopping conduction
- (3) Ohmic conduction
- (4) Space charge-limited conduction
- (5) Ionic conduction
- (6) Grain-boundary-limited conduction

2.3.4 Poole-Frenkel Emission

Poole-Frenkel (PF) emission involves a mechanism which is very similar to Schottky emission, whereby the thermal excitation of electrons may emit from traps into the conduction band of the dielectric. PF emission is often observed at high temperature as it is affected by the thermal activation under an electric field. Considering an electron in a trapping center, the Coulomb potential energy of the electron can be reduced by an applied electric field across the

dielectric film. The reduction in potential energy may increase the probability of an electron being thermally excited out of the trap into the conduction band of the dielectric. The current density due to the P-F emission is (Wong & Cheong, 2010):

$$J = q\mu N_c E \exp \left[\frac{-q(\phi_T - \sqrt{qE/\pi\epsilon_i\epsilon_0})}{kT} \right],$$

μ : Electronic drift mobility

N_c : The density of states in the conduction band

$q\phi_T (= \Phi_T)$: The trap energy level

Figure 2.2 and Figure 2.3 illustrated the schematic energy band diagram for PF emission in comparison to SE in a metal-insulator-structure (MIS).

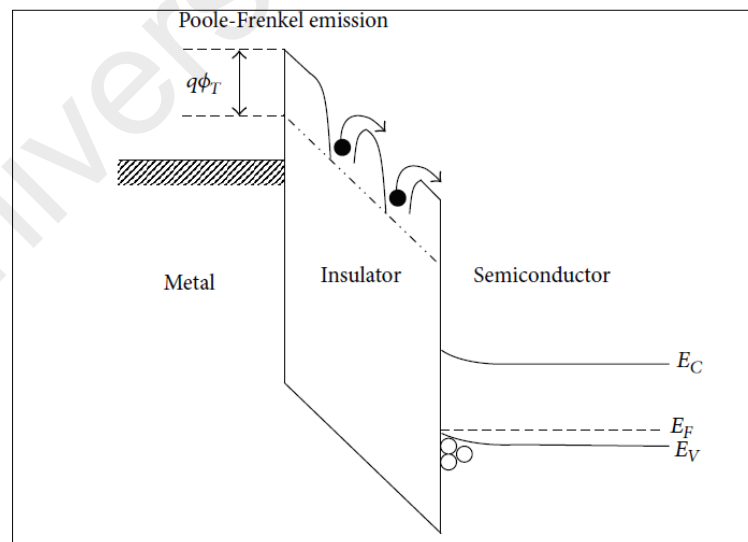


Figure 2.2: Schematic Energy Band Diagram of Poole-Frenkel emission in MIS (Chiu, 2014)

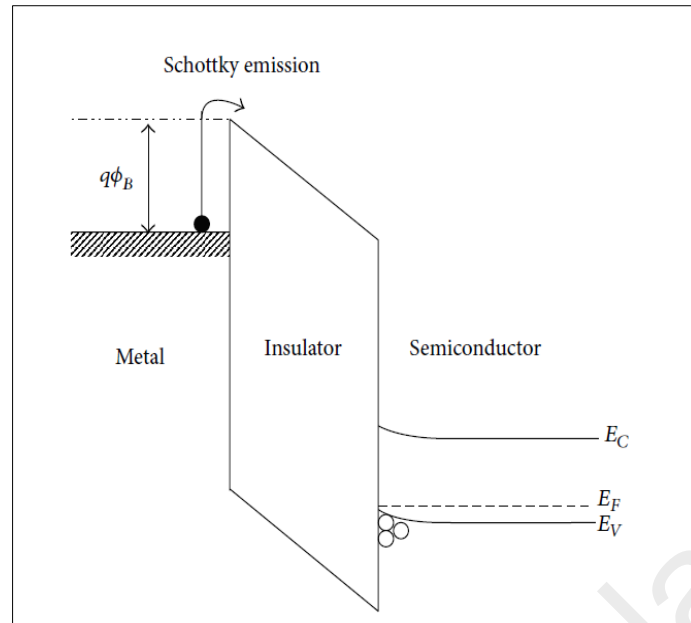


Figure 2.3: Schematic Energy Band Diagram of Schottky emission in MIS (Chiu, 2014)

University of Malaya

CHAPTER 3: METHODOLOGY

3.1 Introduction

Chapter 3 mainly focused on the materials and methodology of the project and the processing route to prepare Zr-oxynitride thin film on SiC substrate. Additionally, this chapter will also discuss about the characterizations of the sample.

In general, Zr-oxynitride thin film on SiC substrate can be formed by simultaneous oxidation and nitridation in nitrous oxide sputtered Zr on SiC. The oxidation and nitridation of the sputtered Zr on SiC substrate were carried out in nitrous oxide ambient for 15 minutes at various temperatures (400°C - 900°C). The effect of temperature on the type of conduction mechanism were studied and investigated. Basically, the experiment involved three main stages which are:

- I. SiC Substrate preparation
- II. Formation of Zr-oxynitride thin film on SiC substrate
- III. Characterization and testing

3.2 Experimental Flow Chart

The methodology adopted in this research work can be summarized in the flow chart shown in Figure 3.1.

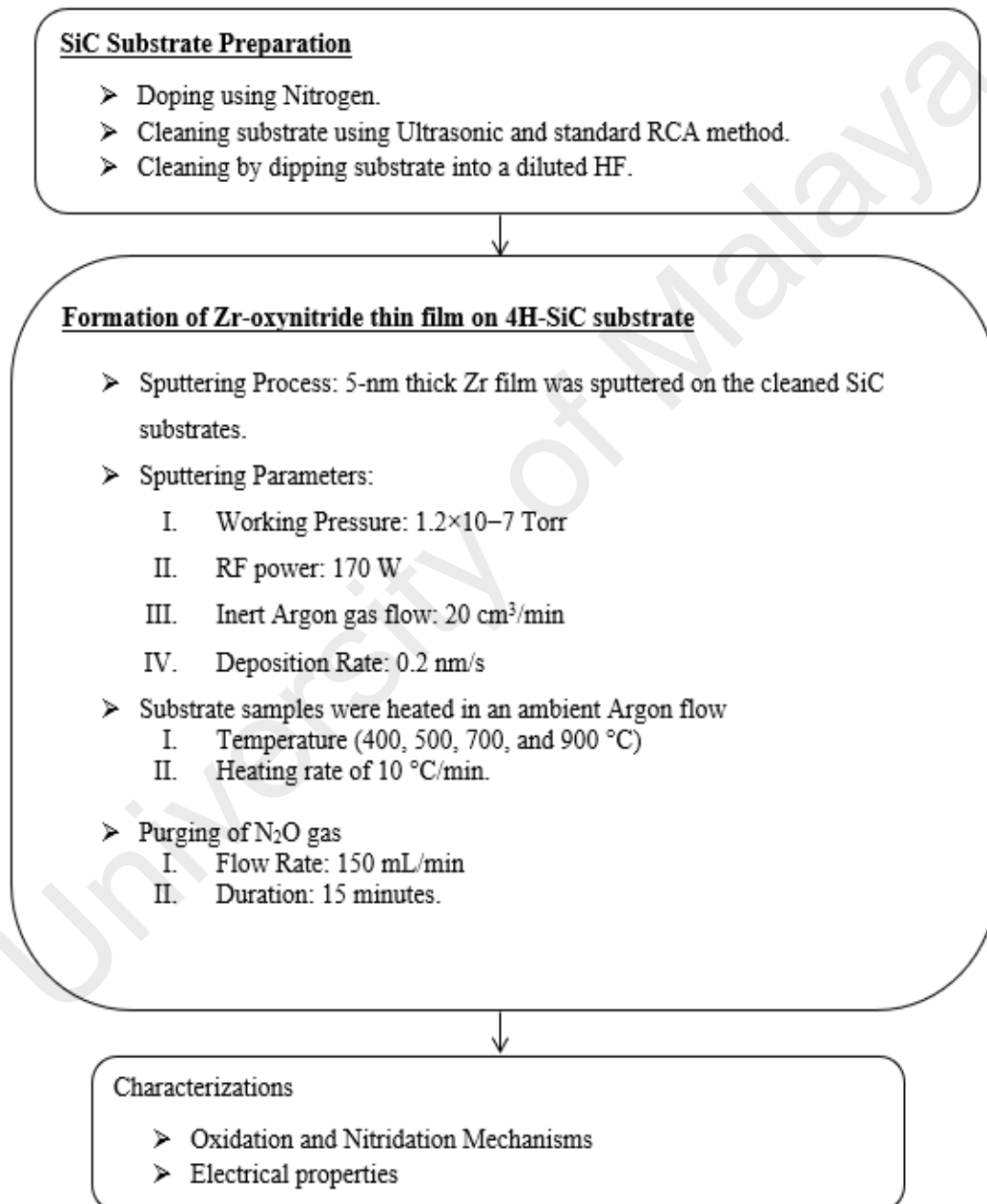


Figure 3.1 : Experimental Flow Chart (Wong & Cheong, 2011)

3.3 Starting Materials

The chemicals used in the research are (Wong & Cheong, 2011):

- I. 0.8 cm × 0.8 cm pre-cut, n-type, (0001) oriented, Si-faced 4H-SiC wafers with 4.09°-off axis, 0.020 Ω cm of resistivity, and 1-μm thick of n-type epitaxial layer.
- II. Nitrogen at concentration of $(1-4) \times 10^{16} \text{ cm}^{-3}$, which were commercially purchased from CREE Inc. (USA)
- III. Hydrofluoric Acid (Hf)

3.4 SiC Substrate Preparation

The pre-cut SiC wafers were doped with Nitrogen. Then, the SiC substrate was cleaned using Ultrasonic and standard RCA (Radio Corporation of America) cleaning method. Next, the native oxide on the surface were removed by dipping the substrate into a diluted HF solution (1 HF:50 H₂O).

3.5 Formation of Zr-Oxynitride Thin Film on SiC Substrate

A 5-nm thick Zr film was deposited on the cleaned SiC substrates by a RF sputtering system (Edwards Auto 500). During the sputtering, working pressure, RF power, inert Argon gas flow, and deposition rate were regulated at 1.2×10^{-7} Torr, 170 W, 20 cm³/min, 0.2 nm/s,

respectively. Samples were placed inside a horizontal tube furnace and heated up from room temperature to a set of temperatures (400, 500, 700, and 900 °C) in an ambient Argon flow with a heating rate of 10 °C/min. Once the set temperature was reached, Argon gas was turned off and N₂O gas was then purged in with a flow rate of 150 mL/min for 15 min. The samples were eventually taken out at room temperature after the furnace was cooled down to room temperature in ambient Ar.

3.6 Characterization and Testing

3.6.1 Electrical Properties

To characterize the electrical properties of the film, Al-gate MOS capacitors with photolithographically defined square area of $9 \times 10^{-4} \text{ cm}^2$ (0.03 cm × 0.03 cm) were fabricated on top of the films. Al film was also deposited on back side of the SiC substrate after removal of native oxide. High frequency (1 MHz) capacitance-voltage (*C-V*) and current-voltage (*I-V*) measurements were conducted by a computer-controlled Agilent HP4284 LCR meter and HP4155-6C semiconductor parameter analyzer (SPA), respectively.

CHAPTER 4: RESULTS & DISCUSSION

4.1 Oxidation and Nitridation Mechanisms

The oxidation and nitridation mechanism of sputtered Zr on SiC substrate using N₂O gas at various temperatures (400, 500, 700 and 900 °C) can be reasoned based on the chemical analysis that had been carried out by XPS. The oxidation of Zr at room temperature had resulted in the formation of a very thin monolayer (~ 1 nm) of ZrO₂ on the top-most surface according to the following reaction (Wong & Cheong, 2012):



According to Miller and Grassian, the decomposition of N₂O above 350 °C can be assisted by using ZrO₂ as the catalyst. At 400 °C, the Zr cations will aid N₂O to decompose into N and O compounds whereby the oxygen atoms will be absorbed by Zr metal. Consequently, the absorbed O atoms may react with Zr to form Zr-O compound. The reaction is described by (Wong & Cheong, 2012):



Where the arrow pointing to the right above a chemical symbol indicates an inward diffusion process of the particular chemical. When a sufficiently high oxygen concentration is provided, a stoichiometric Zr–O (ZrO₂) is formed. When the Zr–O (ZrO₂) thickness increases, less oxygen can disperse in and cause an incomplete Zr–O reaction. As a consequence, a sub-stoichiometric Zr–O compound is formed between the stoichiometric Zr–O (ZrO₂) compound and the SiC substrate towards the interfacial layer. At the same time, the nitridization process occurs. Because N atoms are smaller than O atoms, they can diffuse more quickly than O atoms at the same temperature and duration of processing. Thus, N atoms may further diffuse inside and react with sub-stoichiometric Zr–O to form a compound Zr–N by releasing oxygen (Eq. (3)) or by reacting with unreacted Zr to form Zr – N compound (Eq. (4)):



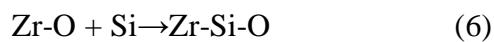
At 500 °C, the formation of ZrN is less desirable than the stoichiometric ZrO₂ formation. For this case, however, the Zr–O involved is sub- or non-stoichiometric, and thus the composition of ZrN (Eqs (3) and (4)) is more desirable.

The formed Zr–N compound can be incorporated into the Zr–O layer towards the interfacial layer. Therefore, Zr-oxynitride layer consisting of Zr–O and Zr–N was established, with Zr–O rich compound situated at the topmost surface and Zr–N rich compound located near the interface region. The released O atoms from the formation of the Zr–N compound (Eq. (4)) and the inward diffusion of O atoms from the ambient may react with the unreacted Zr and

bridge to the top Si layer (dangling Si bonds) of the bulk-terminated SiC surface, thus forming the Zr–Si–O compound:



On the other hand, the formation of Zr–Si–O compound can also be attained through the reaction between the O atoms in the sub-stoichiometric Zr–O and the Si if the bulk-terminated SiC surface.



At a reasonable temperature of 500 °C, Wong & Cheong (2012) stated that the mixture of sub-stoichiometric Zr-O and Zr-N compounds will try to exchange and balance the O and N atoms among each other as a means to attain the thermodynamic equilibrium state. As a result, the compound Zr-O-N is formed. Furthermore, the Zr-O-N compound can also be formed from the diffusion of N atoms from the ambient nitrous oxide gas into the stoichiometric Zr–O (ZrO₂) region.

4.2 Electrical Characterizations

4.2.1 Current Density-Electric Field (J-E) Characteristics and Charge Conduction Mechanisms

Temperature-dependence of leakage currents was investigated to clarify charge conduction mechanisms of the studied samples with Zr thin film being oxidized and nitride for 15 minutes. According to Wong and Cheong (2011), an oxide thickness of 10 nm and K_{eff} value of 21.82 can be obtained when the Zr thin film undergoes sputtering process via N_2O gas for 15 minutes. The leakage currents were measured at different temperatures (400, 500, 700 and 900 °C) respectively. The leakage current density-electric field (J-E) characteristics of all tested samples were obtained by transforming the current-voltage (I-V) measurements obtained from the computer-controlled SPA system. The E value was assessed by (Wong & Cheong, 2011):

$$E = (V_g - V_{\text{FB}})/t_{\text{ox}} \quad (7)$$

In this study, the Schottky emission (SE) and Poole-Frenkel (PF) emission charge mechanism have been considered for the possible charge conduction mechanism of ZrON/SiC material. SE is a field-assisted thermionic emission of an electron over a surface barrier. Figure 4.1 indicate the J-E plot measured at different temperatures for 15 minutes oxidized/nitrided sample fitted by linear extrapolation. Based on the linear fitting, the obtained r^2 was ranged 0.90–0.98. This shows that the data are comply with the standard SE model. The highest values

of ϕ_B (1.19 eV) were achieved. Both ϕ_B and k_r values reduce as the measured temperature increases, as shown in Figure 4.2 and Figure 4.3, respectively.

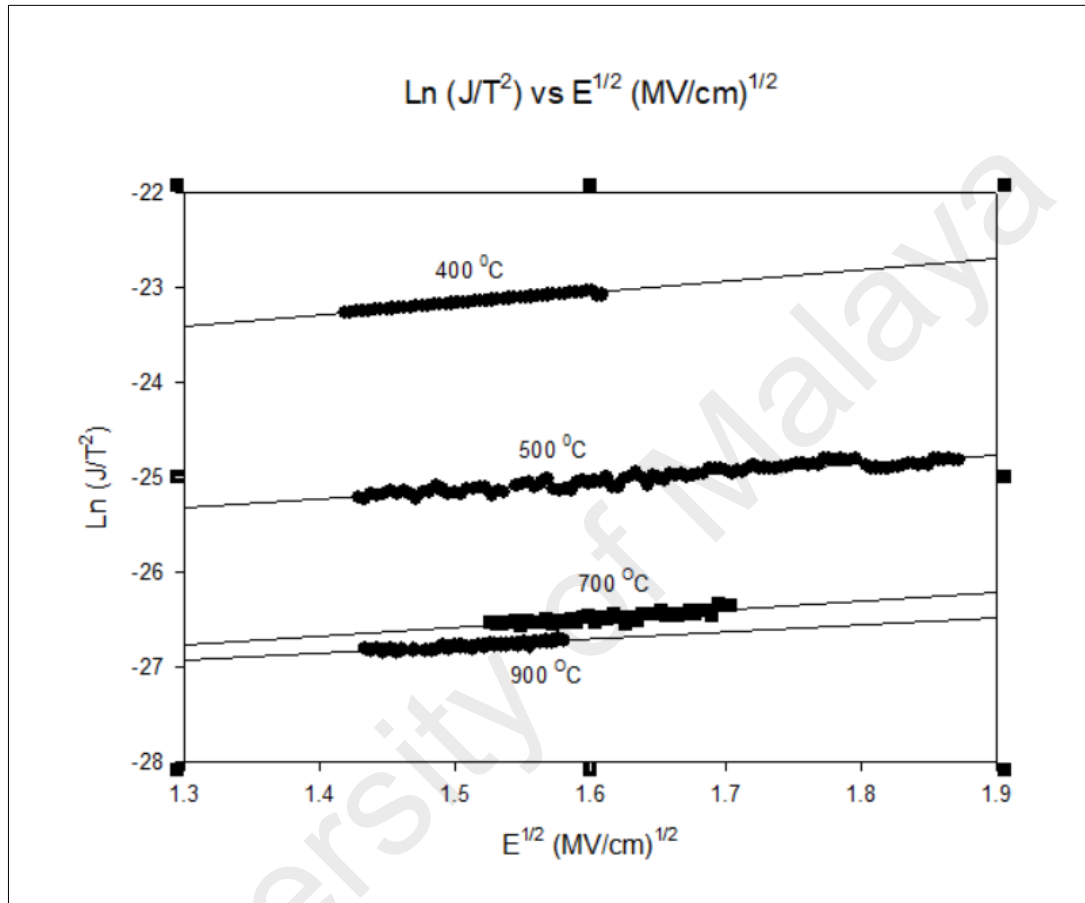


Figure 4.1 : SE Plot (J-E Plot Measured at Different Temperatures for 15 minutes)

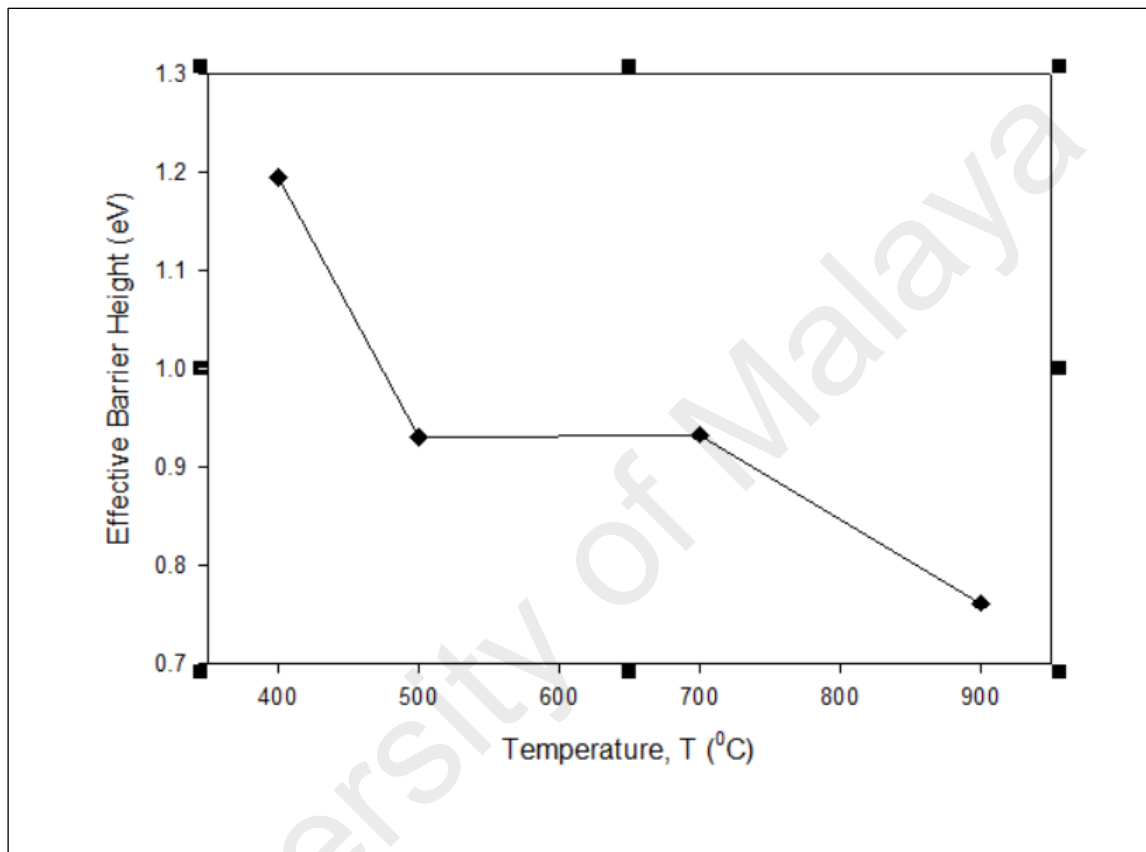


Figure 4.2 : Effective Barrier Height Extracted from SE plot

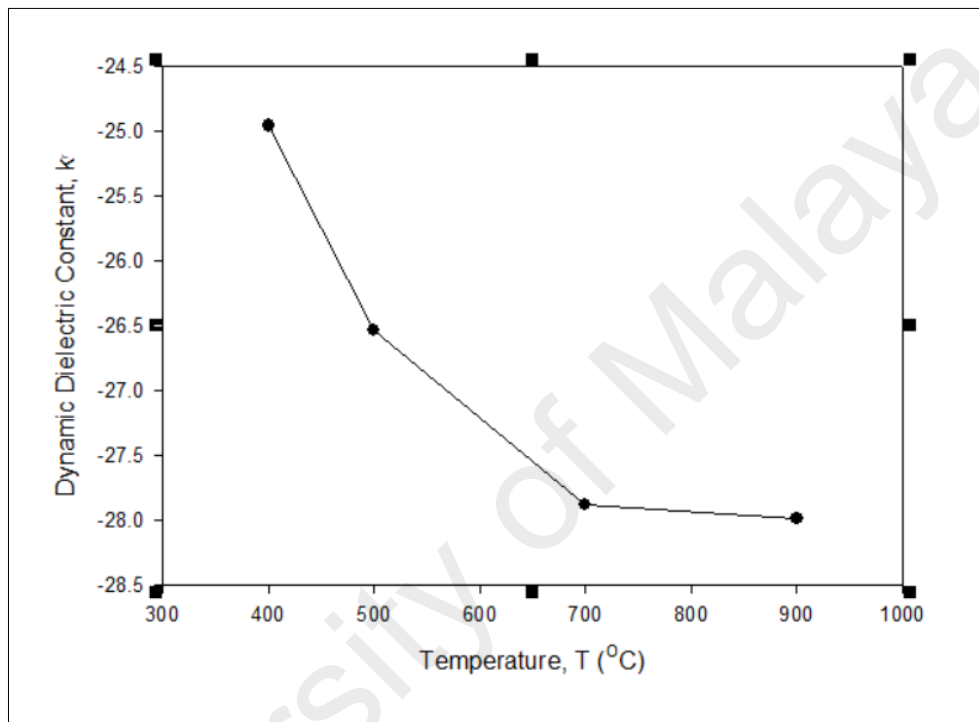


Figure 4.3 : Dynamic Dielectric Constant Extracted from SE Plot

Figure 4.4 shows the measured J-E data and the modelled PF emission curves for ZrON/SiC system. Experimental results showed that the refractive index obtained by the electrical method is extremely close to the one obtained by the optical measurement, with r^2 of 0.90-0.99. This also shows that the data are comparable with the standard PF emission model. Figure 4.5 indicate the sample with temperature of 500 °C has the highest k_f value which is 3.03.

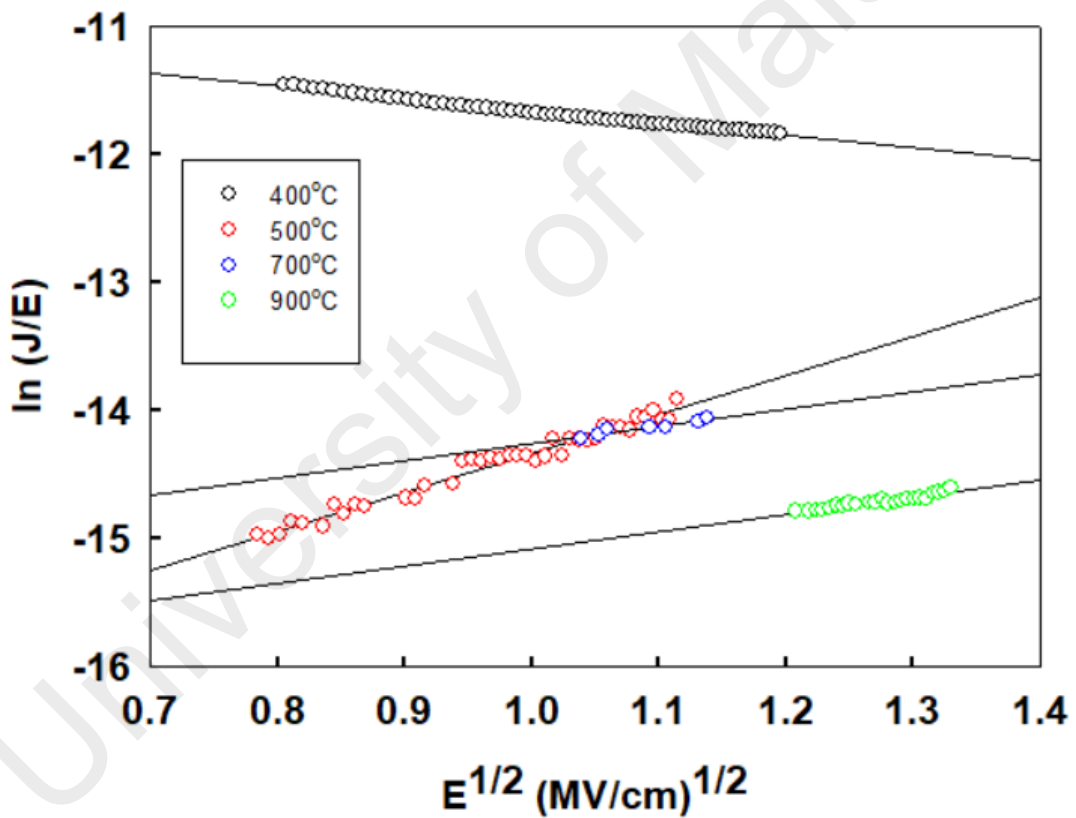


Figure 4.4 : The measured J-E Data and Modelled PF Emission Curves for ZrON/SiC System

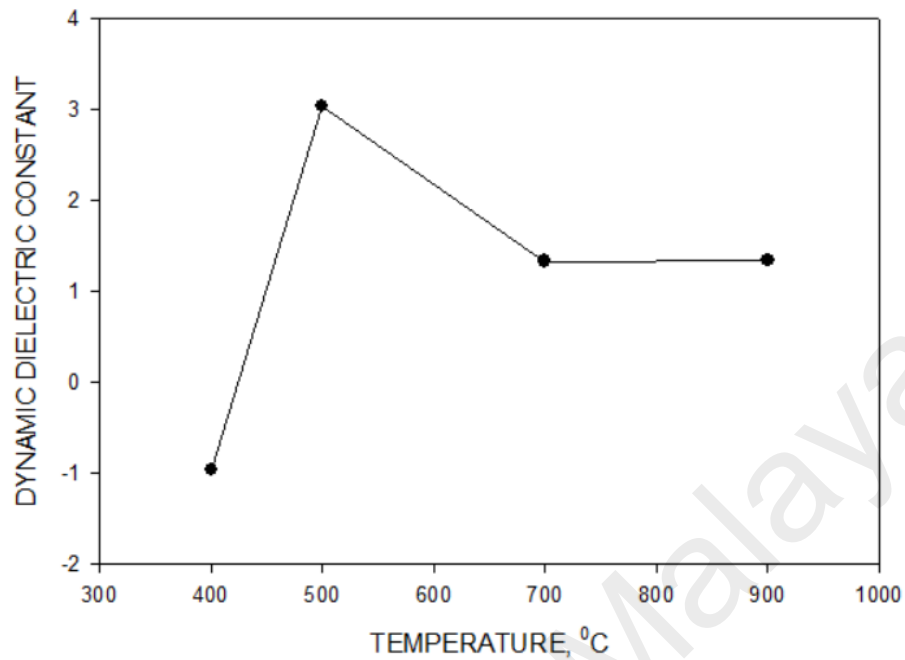


Figure 4.5 : Dynamic Dielectric Constant Extracted versus Temperature based on PF Emission Plot

Table 4.1 are the summarized k_r values obtained from the Gradient $\ln(J/E) - E^{1/2}$ Plot Fitted with Poole-Frenkel Emission as a Function of Oxidation and Nitridation Temperature.

Table 4.1 : Dynamic Dielectric Constant from Gradient $\ln(J/E) - E^{1/2}$ Plot Fitted with Poole-Frenkel Emission as a Function of Oxidation and Nitridation Temperature

Temperature	Dynamic Dielectric Constant, k_r
400 °C	-0.97
500 °C	3.03
700 °C	1.35
900 °C	1.33

In the nutshell, based on both k_r values obtained from the SE and PF graph, it can be agreed upon that the value of k_r decreases as the measured temperature rises. Thus, it is proven that the dielectric constant value declines as the IL thickness increases.

Figure 4.6 shows the relationship between the leakage current density and the electrical field (J-E curve). Based on Figure 4.6, it is observed that the gate oxides experienced dielectric breakdown (E_B) due to instantaneous increment of leakage current density at a specific field. As the temperature increase, the dielectric breakdown decreased. The E_B recorded for sample oxidized/nitrided at 400°C, 500°C, 700°C and 900°C are 4.59 MV/cm, 5.05 MV/cm, 4.16 MV/cm and -0.07 MV/cm respectively. For this study, sample oxidized/nitride at 500°C has the highest E_B . Furthermore, it can be seen that after a certain stage of reaching electrical breakdown at a lower order of magnitude, the sample underwent breakdown at a higher order of magnitude, which is when Fowler-Nordheim (F-N) tunneling occurred, but there was still another conduction mechanism in the process of breaking down before reaching F-N tunneling.

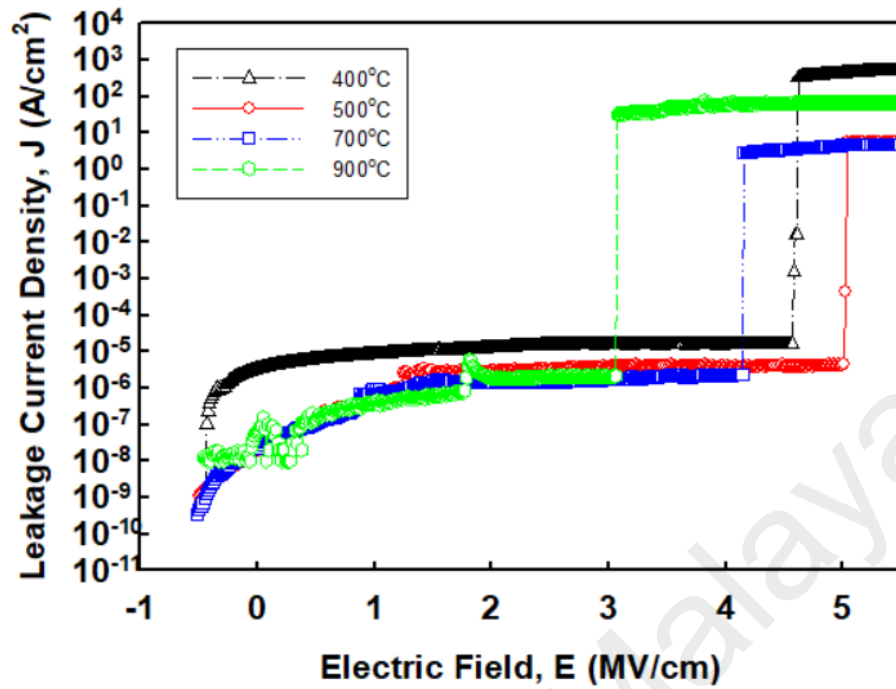


Figure 4.6 : Relationship between Leakage Current Density and Electrical Field for Various Temperature within the Range of 400⁰C – 900⁰C

Samples were oxidized/nitride at 400 °C was the sample that shows the possibility to have other conduction mechanisms before reaching F-N, and this may be known as PF conduction. Reason being PF is the last stage of conduction mechanism that often happened after Ohmic conduction, Child's law, and Schottky or thermionic emission. Thus, this is why only temperature of 400 °C the showed a negative gradient.

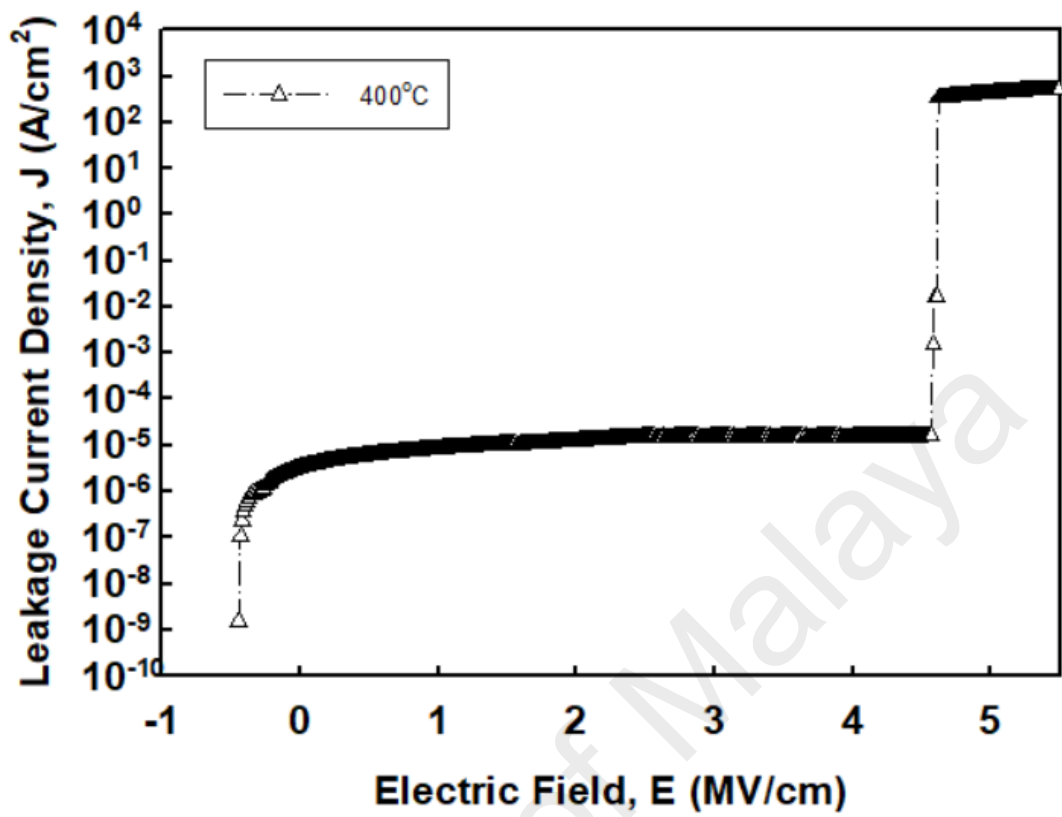


Figure 4.7 : Relationship between Leakage Current Density and Electrical Field for Temperature at 400 °C

CHAPTER 5: CONCLUSION

5.1 Summary

In general, the most commonly described conduction mechanisms for high- k dielectrics are Schottky and Poole–Frenkel (PF) emissions, which are highly temperature-dependent. The electrical properties of the gate oxide are critical to the formation of the conductive channel region below the gate. Overstressing the gate oxide layer, a common failure mode of MOS devices, may lead to gate rupture or to stress induced leakage current. Based on the data tabulated, it can be concluded that the increase in temperature will increase the interfacial layer (IL), which consequently will lead to a reduction in dielectric strength.

5.2 Recommendations for Future Project

- I. Conduction mechanism other than SE and PF emission can be considered. For example, F-N tunneling, Ohmic conduction, space charge-limited conduction and etc.
- II. Different type of gate oxide can be paired with SiC semiconductor instead of ZrON.

LIST OF PUBLICATIONS AND PAPERS PRESENTED

Published works as well as papers presented at conferences, seminars, symposiums etc pertaining to the research topic of the research report/ dissertation/ thesis are suggested be included in this section. The first page of the article may also be appended as reference.

University of Malaya

REFERENCES

- Baliga, J. B. (2018). *Fundamentals of Power Semiconductor Devices* (2nd ed.). Springer.
- Busch, B. W., Schulte, W. H., Garfunkel, E., Gustafsson, T., Qi, W., Nieh, R., & Lee, J. (2000). Oxygen exchange and transport in thin zirconia films on Si(100). *Physical Review B*, 62(20), R13290–R13293. <https://doi.org/10.1103/physrevb.62.r13290>
- Chenari, H. M., Sedghi, H., Talebian, M., Golzan, M. M., & Hassanzadeh, A. (2011). Poole-Frenkel Conduction in Cu/Nano-SnO₂/Cu Arrangement. *Journal of Nanomaterials*, 2011, 1–4. <https://doi.org/10.1155/2011/190391>
- Chiu, F.-C., Lee, C.-Y., & Pan, T.-M. (2009). Current conduction mechanisms in Pr₂O₃/oxynitride laminated gate dielectrics. *Journal of Applied Physics*, 105(7), 074103. <https://doi.org/10.1063/1.3103282>
- Chiu, F. C. (2014). A review on conduction mechanisms in dielectric films. *Advances in Materials Science and Engineering*, 2014. <https://doi.org/10.1155/2014/578168>
- Choyke, W. J., Matsunami, H., & Pensl, G. (2013). *Silicon Carbide*. Springer Publishing.
- Davis, R. F. (2017). Silicon Carbide. *Reference Module in Materials Science and Materials Engineering*, 1–6. <https://doi.org/10.1016/b978-0-12-803581-8.02445-0>
- Feng, Z. C. (2013). *SiC Power Materials: Devices and Applications (Springer Series in Materials Science Book 73)* (2004th ed.). Springer.

- Fraga, M. A., Bosi, M., & Negri, M. (2015). Silicon Carbide in Microsystem Technology — Thin Film Versus Bulk Material. *Advanced Silicon Carbide Devices and Processing*, 3–10. <https://doi.org/10.5772/60970>
- Gerhardt, R. (2011). *Properties and Applications of Silicon Carbide*. IntechOpen.
- Hudgins, J. L. (2003). Wide and narrow bandgap semiconductors for power electronics: A new valuation. *Journal of Electronic Materials*, 32(6), 471–477. <https://doi.org/10.1007/s11664-003-0128-9>
- Karki, U., & Peng, F. Z. (2018). Precursors of Gate-Oxide Degradation in Silicon Carbide MOSFETs. *2018 IEEE Energy Conversion Congress and Exposition (ECCE)*, 1–5. <https://doi.org/10.1109/ecce.2018.8557354>
- Kim, W.-H., Maeng, W. J., Kim, M.-K., Gatineau, J., & Kim, H. (2011). Electronic Structure of Cerium Oxide Gate Dielectric Grown by Plasma-Enhanced Atomic Layer Deposition. *Journal of The Electrochemical Society*, 158(10), G217. <https://doi.org/10.1149/1.3625611>
- Kimoto, T., & Cooper, J. A. (2014). *Fundamentals of Silicon Carbide Technology: Growth, Characterization, Devices and Applications (Wiley - IEEE)* (1st ed.). Wiley-IEEE Press.
- Levinshtein, M. E., Rumyantsev, S. L., & Shur, M. S. (2001). *Properties of Advanced Semiconductor Materials: GaN, AlN, InN, BN, SiC, SiGe* (1st ed.). Wiley-Interscience.

- Marckx, D. A., Llc., P. P., National Renewable Energy Laboratory (U.S.), National Renewable Energy Laboratory (U.S.), Power, P., & United States. Department of Energy. Office of Scientific and Technical Information. (2006). *Breakthrough in Power Electronics from SiC*. National Renewable Energy Laboratory. <https://doi.org/10.2172/881313>
- Millan, J., Godignon, P., Perpina, X., Perez-Tomas, A., & Rebollo, J. (2014). A Survey of Wide Bandgap Power Semiconductor Devices. *IEEE Transactions on Power Electronics*, 29(5), 2155–2163. <https://doi.org/10.1109/tpel.2013.2268900>
- Nieh, R. E., Chang Seok Kang, Hag-Ju Cho, Onishi, K., Rino Choi, Krishnan, S., Jeong Hee Han, Young-Hee Kim, Akbar, M. S., & Lee, J. C. (2003). Electrical characterization and material evaluation of zirconium oxynitride gate dielectric in TaN-gated NMOSFETs with high-temperature forming gas annealing. *IEEE Transactions on Electron Devices*, 50(2), 333–340. <https://doi.org/10.1109/ted.2002.808531>
- Singh, R. (2006). Reliability and performance limitations in SiC power devices. *Microelectronics Reliability*, 46(5–6), 713–730. <https://doi.org/10.1016/j.microrel.2005.10.013>
- Wang, F., Zhang, Z., & Jones, E. A. (2018). *Characterization of Wide Bandgap Power Semiconductor Devices*. Institution of Engineering and Technology.
- Wondrak, W., Held, R., Niemann, E., & Schmid, U. (2001). SiC devices for advanced power and high-temperature applications. *IEEE Transactions on Industrial Electronics*, 48(2), 307–308. <https://doi.org/10.1109/41.915409>

Wong, Y. H., & Cheong, K. Y. (2011b). Electrical Characteristics of Oxidized/Nitrided Zr Thin Film on Si. *Journal of The Electrochemical Society*, 158(12), 1270–1278. <https://doi.org/10.1149/2.106112jes>

Wong, Y. H., & Cheong, K. Y. (2012). Metal-Oxide-Semiconductor Characteristics of Zr-Oxynitride Thin Film on 4H-SiC Substrate. *Journal of The Electrochemical Society*, 159(3), H293–H299. <https://doi.org/10.1149/2.081203jes>

University of Malaya